March 2013

Sediment Profile Imaging Report

Demonstration of *in-situ* Treatment of Contaminated Sediments with Reactive Amendments: Post-Cap Survey #1




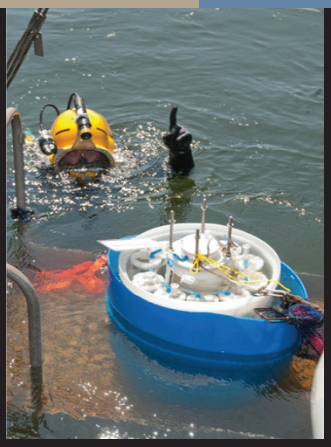


Prepared for

Hart Crowser, Inc.
1700 Westlake Avenue North
Suite 200
Seattle, WA 98109-3856

Hart Crowser Job Number 1789700,
Work Order #1

Prepared by

Germano & Associates, Inc.
12100 SE 46th Place
Bellevue, WA 98006

Sediment Profile Imaging Report

DEMONSTRATION OF *IN-SITU* TREATMENT OF CONTAMINATED SEDIMENTS WITH REACTIVE AMENDMENTS: POST CAP SURVEY #1

Prepared for

Hart Crowser, Inc.
1700 Westlake Avenue North, Suite 200
Seattle, WA 98109-3856

Hart Crowser Job Number 1789700, Work Order #1

Prepared by

Germano & Associates, Inc.
12100 SE 46th Place
Bellevue, WA 98006

March, 2013

TABLE OF CONTENTS

LIST OF FIGURES

1.0
INTRODUCTION

As part of a multidisciplinary effort to investigate the feasibility of treating contaminated sediments in active Department of Defense (DoD) harbors, Germano & Associates, Inc. (G&A) performed a Sediment Profile Imaging (SPI) survey around Pier 7 at the Puget Sound Naval Shipyard & Intermediate Maintenance Facility (PSNS & IMF) Bremerton site. The purpose of this SPI survey was to document conditions at a total of 42 stations following placement of a reactive amendment cap placed on the sediment surface.

2.0
MATERIALS AND METHODS

Between October 14-16, 2012, 141 tons of AquaGate +PAC™ were placed in the target area for remediation under and around Pier 7 at PSNS & IMF Bremerton site (Johnston et al. 2013). Two weeks following cap placement on October 30-31, 2012, scientists from G&A collected a series of sediment profile images at a total of 42[1] stations (Figure 1). Two different versions of an Ocean Imaging Systems Model 3731 sediment profile camera were used for this survey; a standard SPI system using a surrounding frame that was deployed from a vessel (Figure 2), and a hand-held aluminum SPI system (Figure 3) deployed by Navy divers for stations that were located under the pier and inaccessible for sampling with a boat. Stations were arranged in an orthogonal grid of seven rows with six stations in each row, with spacing between stations of approximately 8 meters; half the stations (positions #1, 2, and 3 in each row) were sampled by divers using the hand-held SPI unit, while any remaining stations that were not under the pier (including all of row #7) were sampled from the vessel using the frame-deployed SPI system.

SPI was developed almost four decades ago as a rapid reconnaissance tool for characterizing physical, chemical, and biological seafloor processes and has been used in numerous seafloor surveys throughout North America, Asia, Europe, and Africa (Rhoads and Germano 1982, 1986, 1990; Revelas et al. 1987; Diaz and Schaffner, 1988; Valente et al. 1992; Germano et al. 2011). The sediment profile camera works like an inverted periscope. A Nikon D7000 16.2-megapixel SLR camera with two 8-gigabyte secure digital (SD) cards is mounted horizontally inside a watertight housing on top of a wedge-shaped prism. The prism has a Plexiglas® faceplate at the front with a mirror placed at a 45° angle at the back. The camera lens looks down at the mirror, which is reflecting the image from the faceplate. The prism has an internal strobe mounted inside at the back of the wedge to provide illumination for the image; this chamber is filled with distilled water, so the camera always has an optically clear path. This wedge assembly is mounted on a moveable carriage within a stainless steel frame. The frame is lowered to the seafloor on a winch wire, and the tension on the wire keeps the prism in its "up" position. When the frame comes to rest on the seafloor, the winch wire goes slack (see Figure 2) and the camera prism descends into the sediment at a slow, controlled rate by the dampening action of a hydraulic piston so as not to disturb the sediment-water interface. On the way down, it trips a trigger that activates a time-delay circuit of variable length (operator-selected) to allow the camera to penetrate the seafloor before any image is taken. The knife-sharp edge of the prism transects the sediment, and the prism penetrates the bottom. The strobe is discharged after an appropriate time delay to obtain a cross-sectional image of the upper 20 cm of the sediment column. The resulting images give

1 For the August 2013 survey, an additional transect of SPI stations was added to better delineate the edge of the amended area. These additional stations are shown on this and subsequent figures for future reference

the viewer the same perspective as looking through the side of an aquarium half-filled with sediment. After the first image is obtained at the first location, the camera is then raised up about 2 to 3 meters off the bottom to allow the strobe to recharge; a wiper blade mounted on the frame removes any mud adhering to the faceplate. The strobe recharges within 5 seconds, and the camera is ready to be lowered again for a replicate image. Surveys can be accomplished rapidly by "pogo-sticking" the camera across an area of seafloor while recording positional fixes on the surface vessel.

The hand-held SPI system (Figure 3) works on the same design, except that there is no time delay once the watertight switch is activated by the diver after the prism is inserted into the sediment. There is no wiper blade on the hand-held system, so the diver needs to clean the faceplate of the camera prism manually with a scrub brush after each image is taken.

Two types of adjustments to the SPI system are typically made in the field: physical adjustments to the chassis stop collars on the frame-deployed system or adding/subtracting lead weights to the chassis to control penetration in harder or softer sediments, and electronic software adjustments to the Nikon D7000 to control camera settings. Camera settings (f-stop, shutter speed, ISO equivalents, digital file format, color balance, etc.) are selectable through a water-tight USB port on the camera housing and Nikon Control Pro® software. At the beginning of the survey, the time on both of the sediment profile cameras' internal data loggers was synchronized with the clock on the sampling vessel to local time. Details of the camera settings for each digital image are available in the associated parameters file embedded in the electronic image file; for this survey, the ISO-equivalent was set at 640. The additional camera settings used were as follows: shutter speed was 1/250, f8, white balance set to flash, color mode to Adobe RGB, sharpening to none, noise reduction off, and storage in compressed raw Nikon Electronic Format (NEF) files (approximately 20 MB each). Electronic files were converted to high-resolution jpeg (14-bit) format files (49278 x 3264 pixels) using Nikon Capture NX2® software (Version 2.3.5.).

Three replicate images were taken at each station at the vessel-deployed frame stations, while 2 replicate images were taken by the divers at each of the under-pier stations; each SPI replicate is identified by the time recorded on the digital image file in the camera and in the field log on the vessel. The SD card was immediately surrendered at the completion of the survey to PSNS & IMF for review and approval for public distribution. The unique time stamp on the digital image was then cross-checked with the time stamp recorded in the written sample logs. After the images were cleared by Bremerton security, they were re-named with the appropriate station name based on the time stamp on each image.

Test exposures of the Kodak® Color Separation Guide (Publication No. Q-13) were made on deck at the beginning of the survey to verify that all internal electronic systems were working to design specifications and to provide a color standard against which final

images could be checked for proper color balance. A spare camera and charged battery were carried in the field at all times to insure uninterrupted sample acquisition. After deployment of the camera at each station, the frame counter was checked to make sure that the requisite number of replicates had been taken. In addition, a prism penetration depth indicator on the camera frame was checked to verify that the optical prism had actually penetrated the bottom to a sufficient depth. If images were missed (frame counter indicator or verification from digital download) or the penetration depth was insufficient (penetration indicator), chassis stops were adjusted and/or weights were added or removed, and additional replicate images were taken. Changes in prism weight amounts, the presence or absence of mud doors, and chassis stop positions were recorded for each replicate image.

Following completion of the field operations, the raw NEF image files were converted to high-resolution Joint Photographic Experts Group (jpeg) format files using the minimal amount of image file compression. Once converted to jpeg format, the intensity histogram (RGB channel) for each image was adjusted in Adobe Photoshop® to maximize contrast without distortion. The jpeg images were then imported to Sigmascan Pro® (Aspire Software International) for image calibration and analysis. Calibration information was determined by measuring 1-cm gradations from the Kodak® Color Separation Guide. This calibration information was applied to all SPI images analyzed. Linear and area measurements were recorded as number of pixels and converted to scientific units using the calibration information.

Measured parameters were recorded on a Microsoft® Excel© spreadsheet. G&A's senior scientist (Dr. J. Germano) subsequently checked all these data as an independent quality assurance/quality control review of the measurements before final interpretation was performed.

2.1 MEASURING, INTERPRETING, AND MAPPING SPI PARAMETERS

2.1.1 Prism Penetration Depth

The SPI prism penetration depth was measured from the bottom of the image to the sediment-water interface. The area of the entire cross-sectional sedimentary portion of the image was digitized, and this number was divided by the calibrated linear width of the image to determine the average penetration depth.

Prism penetration is a noteworthy parameter; if the number of weights used in the camera is held constant throughout a survey, the camera functions as a static-load penetrometer. Comparative penetration values from sites of similar grain size give an indication of the relative water content of the sediment. Highly bioturbated sediments and rapidly

accumulating sediments tend to have the highest water contents and greatest prism penetration depths.

The depth of penetration also reflects the bearing capacity and shear strength of the sediments. Overconsolidated or relic sediments and shell-bearing sands resist camera penetration. Highly bioturbated, sulfitic, or methanogenic muds are the least consolidated, and deep penetration is typical. Seasonal changes in camera prism penetration have been observed at the same station in other studies and are related to the control of sediment geotechnical properties by bioturbation (Rhoads and Boyer 1982). The effect of water temperature on bioturbation rates appears to be important in controlling both biogenic surface relief and prism penetration depth (Rhoads and Germano 1982).

2.1.2 Thickness of Depositional Layers

Because of the camera's unique design, SPI can be used to detect the thickness of dredged material and depositional layers (like the reactive amendment). SPI is effective in measuring layers ranging in thickness from 1 mm to 20 cm (the height of the SPI optical window). During image analysis, the thickness of the newly deposited sedimentary layers can be determined by measuring the distance between the pre- and post-disposal sediment-water interface. Recently deposited material is usually evident because of its unique optical reflectance and/or color relative to the underlying material representing the pre-disposal surface. Also, in most cases, the point of contact between the two layers is clearly visible as a textural change in sediment composition, facilitating measurement of the thickness of the newly deposited layer.

2.1.3 Apparent Redox Potential Discontinuity Depth

Aerobic near-surface marine sediments typically have higher reflectance relative to underlying hypoxic or anoxic sediments. Surface sands washed free of mud also have higher optical reflectance than underlying muddy sands. These differences in optical reflectance are readily apparent in SPI images; the oxidized surface sediment contains particles coated with ferric hydroxide (an olive or tan color when associated with particles), while reduced and muddy sediments below this oxygenated layer are darker, generally gray to black (Fenchel 1969; Lyle 1983). The boundary between the colored ferric hydroxide surface sediment and underlying gray to black sediment is called the apparent redox potential discontinuity (aRPD).

The depth of the aRPD in the sediment column is an important time-integrator of dissolved oxygen conditions within sediment porewaters. In the absence of bioturbating organisms, this high reflectance layer (in muds) will typically reach a thickness of 2 mm below the sediment-water interface (Rhoads 1974). This depth is related to the supply rate of molecular oxygen by diffusion into the bottom and the consumption of that oxygen by the sediment and associated microflora. In sediments that have very high

sediment oxygen demand (SOD), the sediment may lack a high reflectance layer even when the overlying water column is aerobic.

In the presence of bioturbating macrofauna, the thickness of the high reflectance layer may be several centimeters. The relationship between the thickness of this high reflectance layer and the presence or absence of free molecular oxygen in the associated porewaters must be considered with caution. The actual RPD is the boundary or horizon that separates the positive reduction potential (Eh) region of the sediment column from the underlying negative Eh region. The exact location of this Eh = 0 boundary can be determined accurately only with microelectrodes; hence, the relationship between the change in optical reflectance, as imaged with the SPI camera, and the actual RPD can be determined only by making the appropriate *in situ* Eh measurements. For this reason, the optical reflectance boundary, as imaged, was described in this study as the "apparent" RPD and it was mapped as a mean value. In general, the depth of the actual Eh = 0 horizon will be either equal to or slightly shallower than the depth of the optical reflectance boundary (Rosenberg et al., 2001). This is because bioturbating organisms can mix ferric hydroxide-coated particles downward into the bottom below the Eh = 0 horizon. As a result, the mean aRPD depth can be used as an estimate of the depth of porewater exchange, usually through porewater irrigation (bioturbation). Biogenic particle mixing depths can be estimated by measuring the maximum and minimum depths of imaged feeding voids in the sediment column. This parameter represents the particle mixing depths of head-down feeders, mainly polychaetes.

The rate of depression of the aRPD within the sediment is relatively slow in organic-rich muds, on the order of 200 to 300 micrometers per day; therefore this parameter has a long time constant (Germano and Rhoads 1984). The rebound in the aRPD is also slow (Germano 1983). Measurable changes in the aRPD depth using the SPI optical technique can be detected over periods of 1 or 2 months. This parameter is used effectively to document changes (or gradients) that develop over a seasonal or yearly cycle related to water temperature effects on bioturbation rates, seasonal hypoxia, SOD, and infaunal recruitment. Time-series RPD measurements following a disturbance can be a critical diagnostic element in monitoring the degree of recolonization in an area by the ambient benthos (Rhoads and Germano 1986).

The mean aRPD depth also can be affected by local erosion. The peaks of disposal mounds commonly are scoured by divergent flow over the mound. This scouring can wash away fines and shell or gravel lag deposits, and can result in very thin surface oxidized layer. During storm periods, erosion may completely remove any evidence of the aRPD (Fredette et al. 1988).

Another important characteristic of the aRPD is the contrast in reflectance at this boundary. This contrast is related to the interactions among the degree of organic loading, the bioturbation activity in the sediment, and the concentrations of bottom-water dissolved oxygen in an area. High inputs of labile organic material increase SOD and,

subsequently, sulfate reduction rates and the associated abundance of sulfide end products. This results in more highly reduced, lower-reflectance sediments at depth and higher aRPD contrasts. In a region of generally low aRPD contrasts, images with high aRPD contrasts indicate localized sites of relatively large inputs of organic-rich material such as phytoplankton, other naturally-occurring organic detritus, dredged material, or sewage sludge.

Because the determination of the aRPD requires discrimination of optical contrast between oxidized and reduced particles, it is difficult, if not impossible, to determine the depth of the aRPD in well-sorted sands of any size that have little to no silt or organic matter in them (Painter et al, 2007). When using SPI technology on sand bottoms, little information other than grain-size, prism penetration depth, and boundary roughness values can be measured; while oxygen has no doubt penetrated the sand beneath the sediment-water interface just due to physical forcing factors acting on surface roughness elements (Ziebis et al., 1996; Huettel et al., 1998), estimates of the mean aRPD depths in these types of sediments are indeterminate with conventional white light photography.

2.1.4 Infaunal Successional Stage

The mapping of infaunal successional stages is readily accomplished with SPI technology. These stages are recognized in SPI images by the presence of dense assemblages of near-surface polychaetes and/or the presence of subsurface feeding voids; both may be present in the same image. Mapping of successional stages is based on the theory that organism-sediment interactions in fine-grained sediments follow a predictable sequence after a major seafloor perturbation. This theory states that primary succession results in "the predictable appearance of macrobenthic invertebrates belonging to specific functional types following a benthic disturbance. These invertebrates interact with sediment in specific ways. Because functional types are the biological units of interest..., our definition does not demand a sequential appearance of particular invertebrate species or genera" (Rhoads and Boyer 1982). This theory is presented in Pearson and Rosenberg (1978) and further developed in Rhoads and Germano (1982) and Rhoads and Boyer (1982).

This continuum of change in animal communities after a disturbance (primary succession) has been divided subjectively into four stages: Stage 0, indicative of a sediment column that is largely devoid of macrofauna, occurs immediately following a physical disturbance or in close proximity to an organic enrichment source; Stage 1 is the initial community of tiny, densely populated polychaete assemblages; Stage 2 is the start of the transition to head-down deposit feeders; and Stage 3 is the mature, equilibrium community of deep-dwelling, head-down deposit feeders (Figure 4).

After an area of bottom is disturbed by natural or anthropogenic events, the first invertebrate assemblage (Stage 1) appears within days after the disturbance. Stage 1 consists of assemblages of tiny tube-dwelling marine polychaetes that reach population

densities of 10^4 to 10^6 individuals per m². These animals feed at or near the sediment-water interface and physically stabilize or bind the sediment surface by producing a mucous "glue" that they use to build their tubes. Sometimes deposited dredged material layers contain Stage 1 tubes still attached to mud clasts from their location of origin; these transported individuals are considered as part of the *in situ* fauna in our assignment of successional stages.

If there are no repeated disturbances to the newly colonized area, then these initial tube-dwelling suspension or surface-deposit feeding taxa are followed by burrowing, head-down deposit-feeders that rework the sediment deeper and deeper over time and mix oxygen from the overlying water into the sediment. The animals in these later-appearing communities (Stage 2 or 3) are larger, have lower overall population densities (10 to 100 individuals per m²), and can rework the sediments to depths of 3 to 20 cm or more. These animals "loosen" the sedimentary fabric, increase the water content in the sediment, thereby lowering the sediment shear strength, and actively recycle nutrients because of the high exchange rate with the overlying waters resulting from their burrowing and feeding activities.

In dynamic estuarine and coastal environments, it is simplistic to assume that benthic communities always progress completely and sequentially through all four stages in accordance with the idealized conceptual model depicted in Figure 3. Various combinations of these basic successional stages are possible. For example, secondary succession can occur (Horn, 1974) in response to additional labile carbon input to surface sediments, with surface-dwelling Stage 1 or 2 organisms co-existing at the same time and place with Stage 3, resulting in the assignment of a "Stage 1 on 3" or "Stage 2 on 3" designation.

While the successional dynamics of invertebrate communities in fine-grained sediments have been well-documented, the successional dynamics of invertebrate communities in sand and coarser sediments are not well-known. Subsequently, the insights gained from sediment profile imaging technology regarding biological community structure and dynamics in sandy and coarse-grained bottoms are fairly limited.

2.1.5 Biological Mixing Depth

During the past two decades, there has been a considerable emphasis on studying the effects of bioturbation on sediment geotechnical properties as well as sediment diagenesis (Ekman et al., 1981; Nowell et al., 1981; Rhoads and Boyer, 1982; Grant et al., 1982; Boudreau, 1986; 1994; 1998). However, an increasing focus of research is centering on the rates of contaminant flux in sediments (Reible and Thibodeaux, 1999; François et al., 2002; Gilbert et al., 2003), and the two parameters that affect the time rate of contaminant flux the greatest are erosion and bioturbation (Reible and Thibodeaux, 1999). The depth to which sediments are bioturbated, or the biological mixing depth, can be an important

parameter for studying either nutrient or contaminant flux in sediments. While the apparent RPD is one potential measure of biological mixing depth, it is quite common in profile images to see evidence of biological activity (burrows, voids, or actual animals) well below the mean apparent RPD. Both the minimum and maximum linear distance from the sediment surface to both the shallowest and deepest feature of biological activity can be measured along with a notation of the type of biogenic structure measured. For this report, the maximum depth to which any biological activity was noted was measured and mapped.

.

3.0
RESULTS

While replicate images were taken at each station, the amount of disturbance caused by the diver-deployed system did not allow for reliable measurements of precision between the two replicate images, so only one replicate (the least disturbed) from each station sampled by divers was analyzed. The amount of debris in and around the piers coupled with the high density of shell fragments also created high variation in the penetration depth at the frame deployed stations, with cross-sectional sedimentary structures masked or destroyed by debris (natural or anthropogenic) being dragged down by the prism cutting blade. While a copy of all images collected was provided to the client, given the variation in image feature preservation (regardless of whether they were taken with the frame-deployed or diver-deployed system), and because this variation in cross-sectional structural appearance was not really indicative of natural variance in the measured parameters, the best image (least disturbed) from each station was analyzed. A complete set of all the summary data measured from each image is presented in Appendix A.

The results for some SPI parameters are sometimes indicated in the data appendix or on the maps as being "Indeterminate" (Ind). This is a result of the sediments being either: 1) too compact for the profile camera to penetrate adequately, preventing observation of surface or subsurface sediment features, 2) too soft to bear the weight of the camera, resulting in over-penetration to the point where the sediment/water interface was above the window (imaging area) on the camera prism (the sediment/water interface must be visible to measure most of the key SPI parameters like aRPD depth, penetration depth, and infaunal successional stage), or 3) the biogenic and sedimentary stratigraphic structure was compromised or destroyed by sampling artifacts caused by the divers inserting the prism into the sediment (either vibrating or wiggling the camera to achieve greater penetration, which allowed suspended sediment to collect in between the cross-sectional profile and the faceplate of the prism)

SPI has been shown to be a powerful reconnaissance tool that can efficiently map gradients in sediment type, biological communities, or disturbances from physical forces or organic enrichment. The results and conclusions in this report are about dynamic processes that have been deduced from imaged structures; as such, they should be considered hypotheses available for further testing/confirmation. By employing Occam's Razor, we feel reasonably assured that the most parsimonious explanation is usually the one borne out by subsequent data confirmation

3.1 PRISM PENETRATION DEPTH

Sediments throughout the site ranged from silt-clays with minor fractions of very fine to fine sand in the rows that ran under the pier, to silty sands as one progressed beyond the pier into Transect #7 (Figure 5). The addition of the AquaGate amendment material to the sediment surface also provided some surface armoring at select stations which impeded camera prism penetration compared to baseline conditions (Figure 6). The mean prism penetration depth in the study area ranged from 4.1 to 20.7 cm, with an overall site average of 14.6 cm; the spatial distribution of mean penetration depth at all stations sampled is shown in Figure 7.

3.2 THICKNESS OF REACTIVE AMENDMENT LAYER

Measureable deposits of AquaGate+PAC^{TM} could be seen at 12 stations, while 7 stations showed only traces of the AquaGate particles in the upper oxidized layer of sediment (Figure 8). At those stations where the cap material could be detected, the average thickness ranged from trace layers to 17.1 cm, with an overall site average of 4.0 cm. The footprint of the cap is shown in Figure 9.

3.3 APPARENT REDOX POTENTIAL DISCONTINUITY DEPTH

The distribution of mean apparent RPD depths is shown in Figure 10; mean aRPD depths could not be measured at 4 of the stations sampled by divers because of sampling artifacts that caused distortions to the sediment profile and eliminated the possibility of any accurate measurements. While twelve of the stations had no detectable aRPD present because of the recent placement of the cap material (see Figure 10), the remaining stations had values ranging from 0.4 to 5.2 cm, with an overall site average of 1.7 cm.

3.4 INFAUNAL SUCCESSIONAL STAGE

The mapped distribution of infaunal successional stages is shown in Figure 11; while there was a noticeable change in biological community status compared to baseline conditions because of the recent disturbance to the area from the cap placement, presence of Stage 3 taxa (infaunal deposit feeders) was evident at 19 of the 42 stations. Three of the stations outboard of the pier (Stations 3-4, 4-4, and 5-4) that formerly had dense assemblages of tubes from large sabellid polychaetes in the baseline survey were now devoid of any of these assemblages after cap placement (Figure 12).

3.5 MAXIMUM BIOLOGICAL MIXING DEPTH

The spatial distribution of the maximum depth to which any biological activity was seen in the study area is shown in Figure 13. Evidence of infaunal burrowing was seen even in some of the images where there was no detectable aRPD due to the high sediment-oxygen demand of the cap amendment; maximum depth of biogenic activity ranged from 0 to 17.3 cm, with an overall site average of 10.5 cm.

4.0
DISCUSSION

As predicted after the baseline survey was completed, we did not have any difficulty detecting the presence of the AquaGate+PAC^{TM} particles in the profile images; even though the SPI survey was conducted only two weeks after the material had been placed, the covering of activated carbon particles had already dissolved off the underlying carrier granules (leaving what looked like white gravel on the sediment surface; see Figure 14) and was being worked into the underlying sediment by the burrowing activities of resident infauna. While some of the stations had the dense colonies of sabellid polychaetes eliminated from the cap placement, future surveys will determine whether or not they re-establish themselves at the 3 locations where they had previously existed but were buried by the capping operations.

The results from this survey showed that the placement of the activated cap amendment did not cover all of the originally targeted placement area with the AquaGate+PACTM material (Figure 15). It is premature at this point to predict whether or not the beneficial effects from the activated cap placement will be as widespread as originally intended.

As noted from the baseline survey, it was still difficult to get accurate measurements of subsurface features from many of the images collected by divers at locations under the pier. We hope that with some additional instructions and having the benefit of the baseline and post-capping results to show the divers, they will be able to improve their "prism insertion" techniques in future monitoring surveys so that the number of sampling artifacts are decreased in the images from under the pier and will allow us to get more accurate measurements of parameters of interest in future monitoring efforts.

5.0
REFERENCES CITED

Boudreau, B.P. 1986. Mathematics of tracer mixing in sediment. I-Spatially-dependent, diffusive mixing. II: Non-local mixing and biological conveyor-belt phenomena. Am. Jour. Sci. 286: 161-238.

Boudreau, B.P. 1994. Is burial velocity a master parameter for bioturbation? Geochimica et Cosmochemica Acta 58: 1243-1249.

Boudreau, B. P. 1998. Mean mixed depth of sediments: The wherefore and the why. Limnol. Oceanogr. 43: 524-526.

Diaz, R. J. and L. C. Schaffner. 1988. Comparison of sediment landscapes in the Chesapeake Bay as seen by surface and profile imaging, p. 222-240 In M. P. Lynch and E. C. Krome (eds.), Understanding the Estuary: Advances in Chesapeake Bay Research, Chesapeake Bay Research Consortium Publication 129, Chesapeake Bay Program 24/88.

Ekman, J.E., Nowell, A.R.M., and P.A. Jumars. 1981. Sediment destabilization by animal tubes. J. Mar. Res. 39: 361-374.

Fenchel, T. 1969. The ecology of marine macrobenthos IV. Structure and function of the benthic ecosystem, its chemical and physical factors and the microfauna communities with special reference to the ciliated protozoa. Ophelia 6: 1-182.

François, F., Gerino, M., Stora, G., Durbec, J.P., and J.C. Poggiale. 2002. Functional approach to sediment reworking by gallery-forming macrobenthic organisms: modeling and application with the polychaete *Nereis diversicolor*. Marine Ecology Progress Series 229: 127–136.

Fredette, T.J., W.F. Bohlen, D.C. Rhoads, and R.W. Morton. 1988. Erosion and resuspension effects of Hurricane Gloria at Long Island Sound dredged material disposal sites. In: Proceedings of the Water Quality ‘88 seminar, February Meeting, Charleston, South Carolina. U.S. Army Corps of Engineers, Hydraulic Engineering Center, Davis, CA.

Germano, J.D. 1983. Infaunal succession in Long Island Sound: Animal-sediment interactions and the effects of predation. Ph.D. dissertation. Yale University, New Haven, CT. 206 pp.

Germano, J.D. and D.C. Rhoads. 1984. REMOTS sediment profiling at the Field Verification Program (FVP) Disposal Site. In: Dredging '84 Proceedings, ASCE, Nov. 14-16, Clearwater, FL. pp. 536-544.

Germano, J.D., D.C. Rhoads, R.M. Valente, D.A. Carey, and M. Solan. 2011. The use of Sediment Profile Imaging (SPI) for environmental impact assessments and monitoring studies – lessons learned from the past four decades. Oceanography and Marine Biology: An Annual Review 49: 247-310.

Gilbert, F. S. Hulth, N. Strömberg, K. Ringdahl, and J.-C. Poggiale. 2003. 2-D optical quantification of particle reworking activities in marine surface sediments. Jour. Exp. Mar. Biol. Ecol. 285-286: 251-264.

Grant, W.D., Jr., Boyer, L.F., and Sanford, L.P. 1982. The effects of bioturbation on the initiation of motion of intertidal sands: Jour. Mar. Res., Vol. 40, pp. 659-677.

Horn, H.S. 1974. The ecology of secondary succession. Ann. Rev. Ecol. Syst. 5: 25-37.

Huettel, M., Ziebis, W., Forster., S., and G.W. Luther III. 1998. Advective transport affecting metal and nutrient distributions and interfacial fluxes in permeable sediments. Geochimica et Cosmochemica Acta 62: 613-631.

Johnston, R.K., V. Kirtay, D.B. Chadwick, G.H. Rosen, J.M. Guerrero, J. Collins, C. Ortega, R. Webb, R,. May, J. Germano, D. Browning, E. Beaver, M. Wicklein, J. Pittz, D.E. Leisle, L. Doyle, and L. Hsu. 2013. Installing an activated-carbon sediment amendment at the Puget Sound Naval Shipyard and Intermediate Maintenance Facility, Bremerton, WA. Paper B-024, Proceedings of the Seventh International Conference on Remediation of Contaminated Sediments (Dallas, TX; February 4-7, 2013). ISBN 978-0-9818730-6-7. ©2013 Battelle Memorial Institute, Columbus, OH. www.battelle.org/sedimentscon

Lyle, M. 1983. The brown-green colour transition in marine sediments: A marker of the Fe (III) – Fe(II) redox boundary. Limnol. Oceanogr. 28: 1026-1033.

Nowell, A.R.M., P.A. Jumars, and J.E. Ekman. 1981. Effects of biological activity on the entrainment of marine sediments. Mar. Geol. 42: 133-153.

Painter, T.H., M. E. Schaepman, W. Schweizer, and J. Brazile. 2007. Spectroscopic discrimination of shit from shinola. Annals of Improbable Research 13: 22-23.

Pearson, T.H. and R. Rosenberg. 1978. Macrobenthic succession in relation to organic enrichment and pollution of the marine environment. Oceanogr. Mar. Biol. Ann. Rev. 16:229-311.

Reible, D and Thibodeaux, L. 1999. Using Natural Processes to Define Exposure From Sediments., in Sediment Management Work Group; Contaminated Sediment Management Technical Papers, Sediment Management Work Group, http://www.smwg.org/index.htm.

Revelas, E.C., J.D. Germano, and D.C. Rhoads. 1987. REMOTS reconnaissance of benthic environments. pp. 2069-2083. In: Coastal Zone '87 Proceedings, ASCE, WW Division, May 26-29, Seattle, WA.

Rhoads, D.C. 1974. Organism-sediment relations on the muddy seafloor. Oceanogr. Mar. Biol. Ann. Rev. 12: 263-300.

Rhoads, D.C. and L.F. Boyer. 1982. The effects of marine benthos on physical properties of sediments. pp. 3-52. In: Animal-Sediment Relations. McCall, P.L. and M.J.S. Tevesz (eds). Plenum Press, New York, NY.

Rhoads, D.C. and J.D. Germano. 1982. Characterization of benthic processes using sediment profile imaging: An efficient method of remote ecological monitoring of the seafloor (REMOTS™ System). Mar. Ecol. Prog. Ser. 8:115-128.

Rhoads, D.C. and J.D. Germano. 1986. Interpreting long-term changes in benthic community structure: A new protocol. Hydrobiologia. 142:291-308.

Rhoads, D.C. and J.D. Germano. 1990. The use of REMOTS® imaging technology for disposal site selection and monitoring. pp. 50-64. In: Geotechnical Engineering of Ocean Waste Disposal, K. Demars and R. Chaney (eds). ASTM Symposium Volume, January, 1989. Orlando, FL.

Rosenberg, R., H.C. Nilsson, and R.J. Diaz. 2001. Response of benthic fauna and changing sediment redox profiles over a hypoxic gradient. Estuarine, Coastal and Shelf Science 53: 343-350.

Valente, R.M., D.C. Rhoads, J.D. Germano, and V.J. Cabelli. 1992. Mapping of benthic enrichment patterns in Narragansett Bay, RI. Estuaries 15:1-17.

Ziebis, W., Huettel, M., and S. Forster. 1996. Impact of biogenic sediment topography on oxygen fluxes in permeable seabeds. Mar. Ecol. Prog. Ser. 140: 227-237.

FIGURES

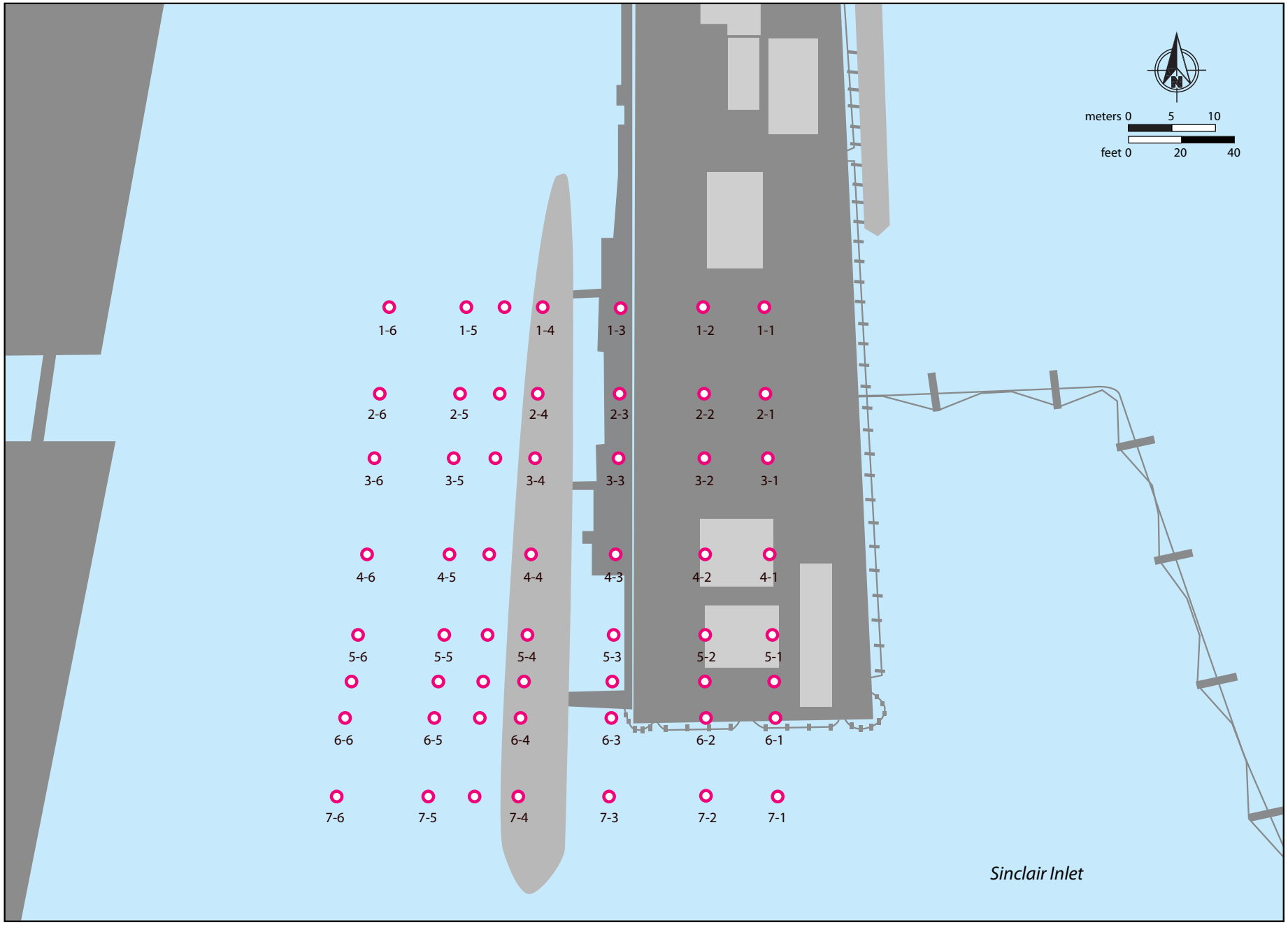

Figure 1: Location of SPI stations under and around Pier 7 at PSNS & IMF, Bremerton site.

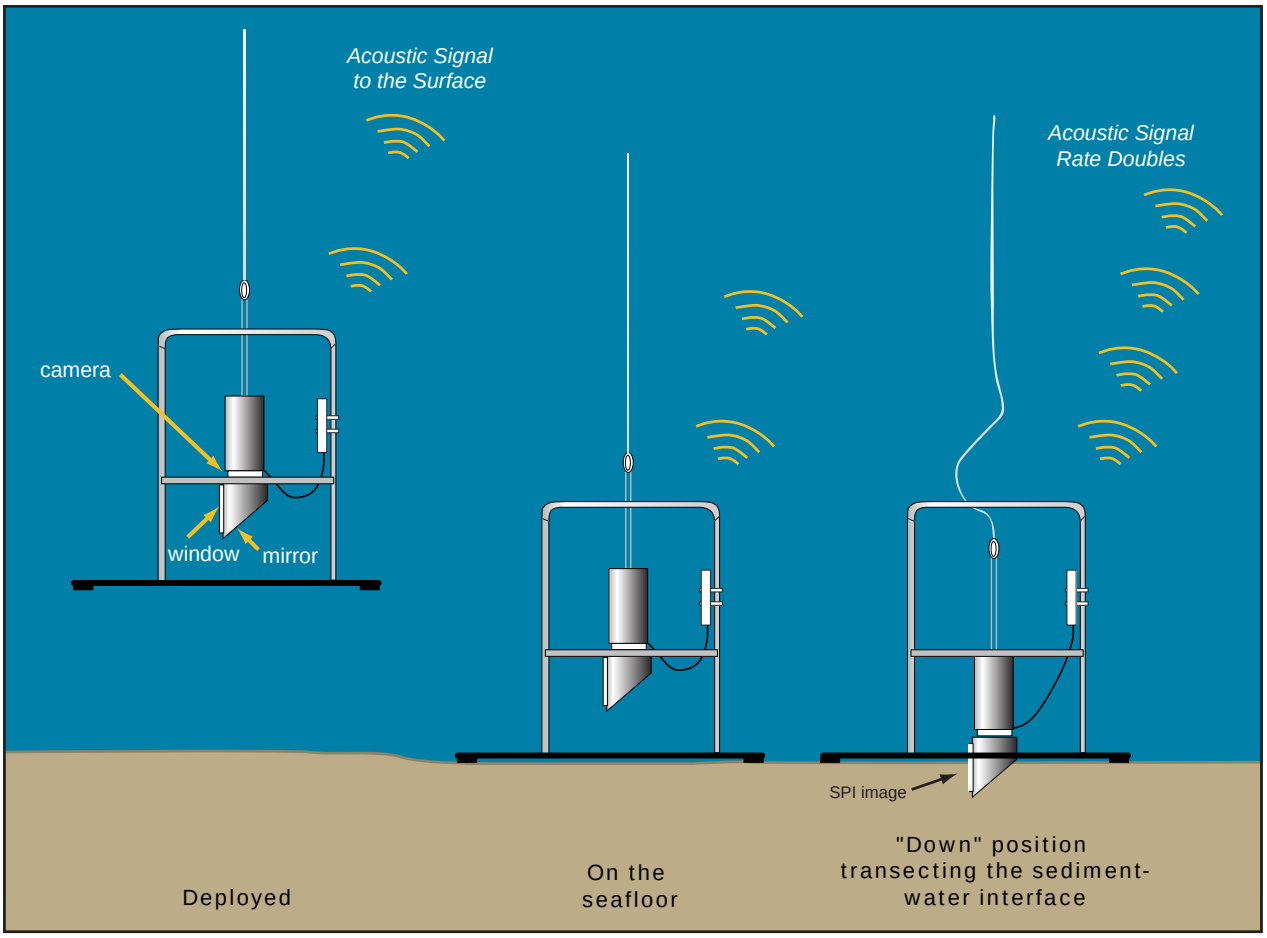

Figure 2: Deployment and operation of the SPI camera system. The central cradle of the camera is held in the “up” position by tension on the winch wire as it is being lowered to the seafloor (left); once the frame base hits the bottom (center), the prism is then free to penetrate the bottom (right) and take the photograph.

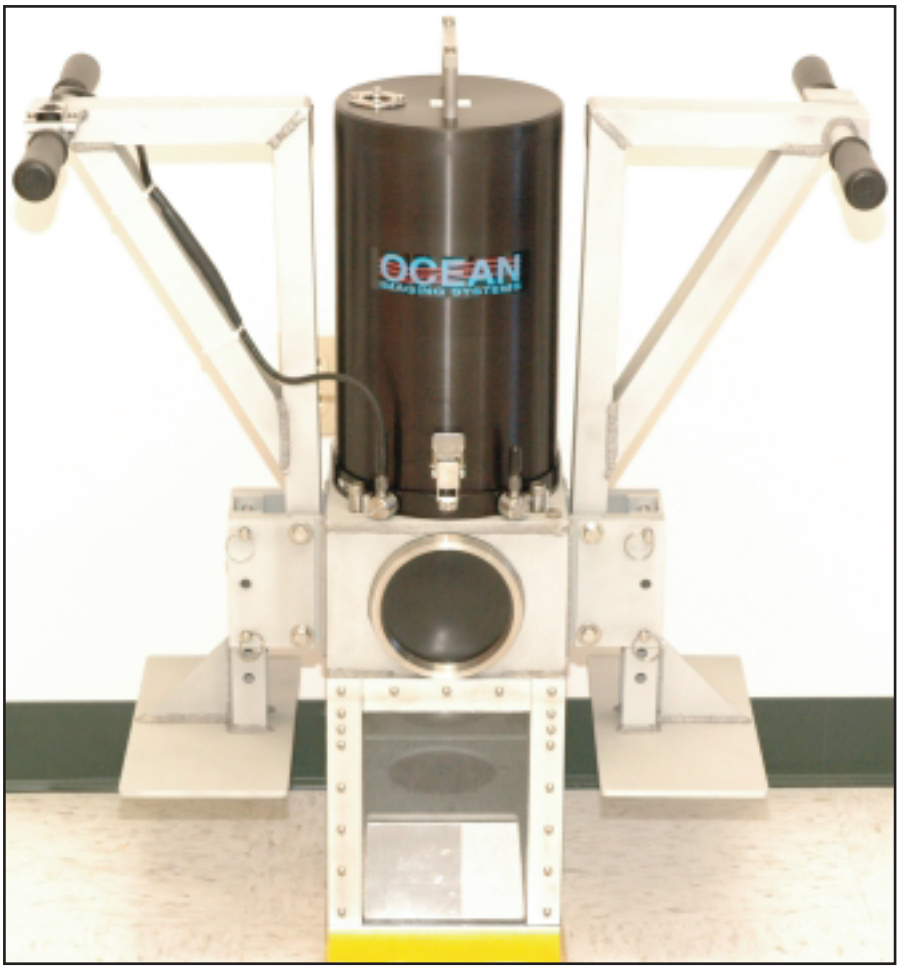

Figure 3: The hand-held SPI system used by divers for all stations that were located underneath Pier 7 at PSNS & IMF, Bremerton site.

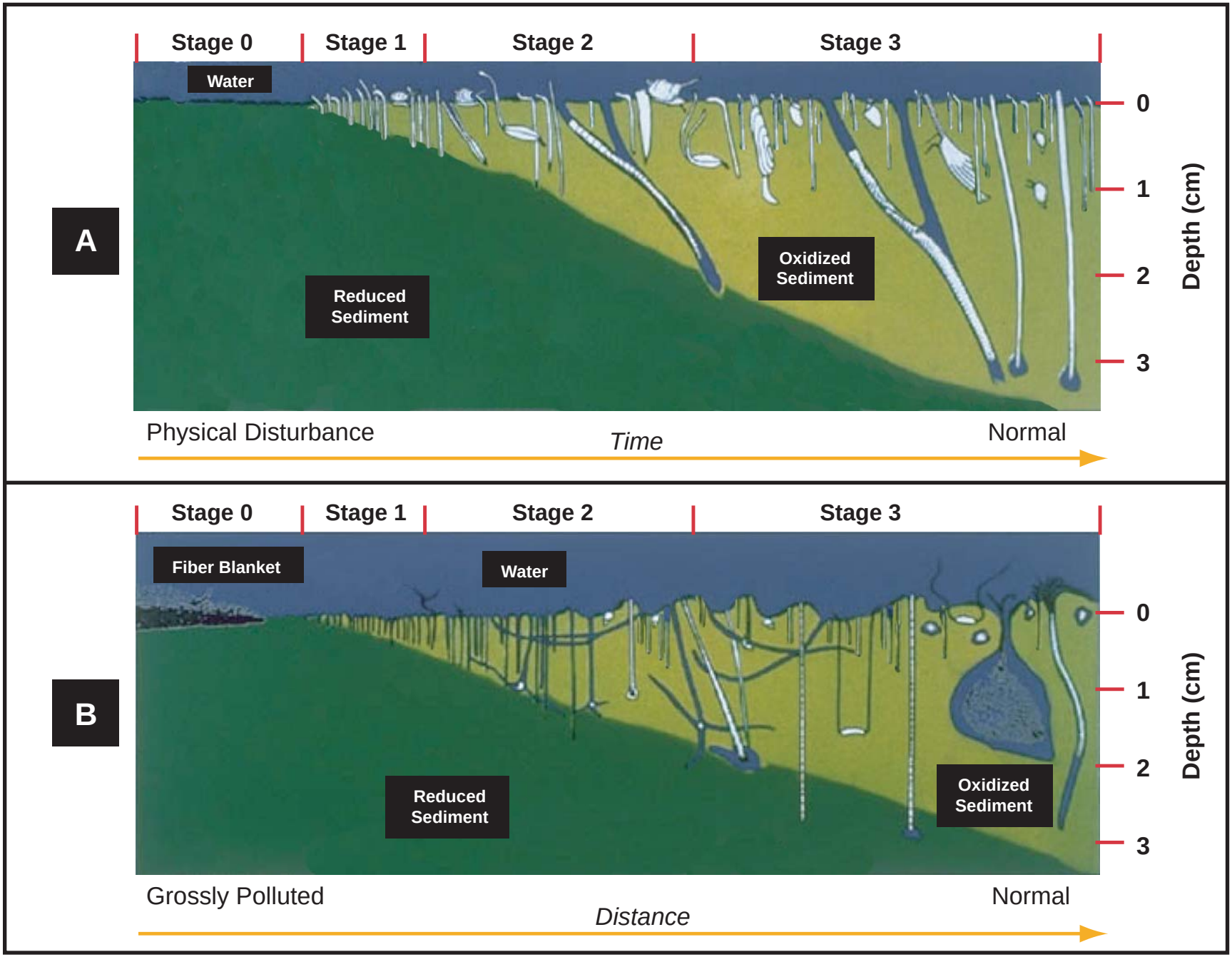

Figure 4: The stages of infaunal succession as a response of soft-bottom benthic communities to physical disturbance (top panel) or organic enrichment (bottom panel). From Rhoads and Germano, 1982.

1-5 7-3

Figure 5: The lower fraction of sand in the natural silt-clay sediments at stations toward the north of the grid allowed for greater prism penetration as seen in this profile image from Station 1-5 (left) as compared with some of the stations south of the pier with a greater fraction of fine to medium sand as seen in this image from Station 7-3 (right). Scale: width of each image = 14.5 cm. Note: Orange band at top of right image is the rubber faceplate-wiper on SPI system.

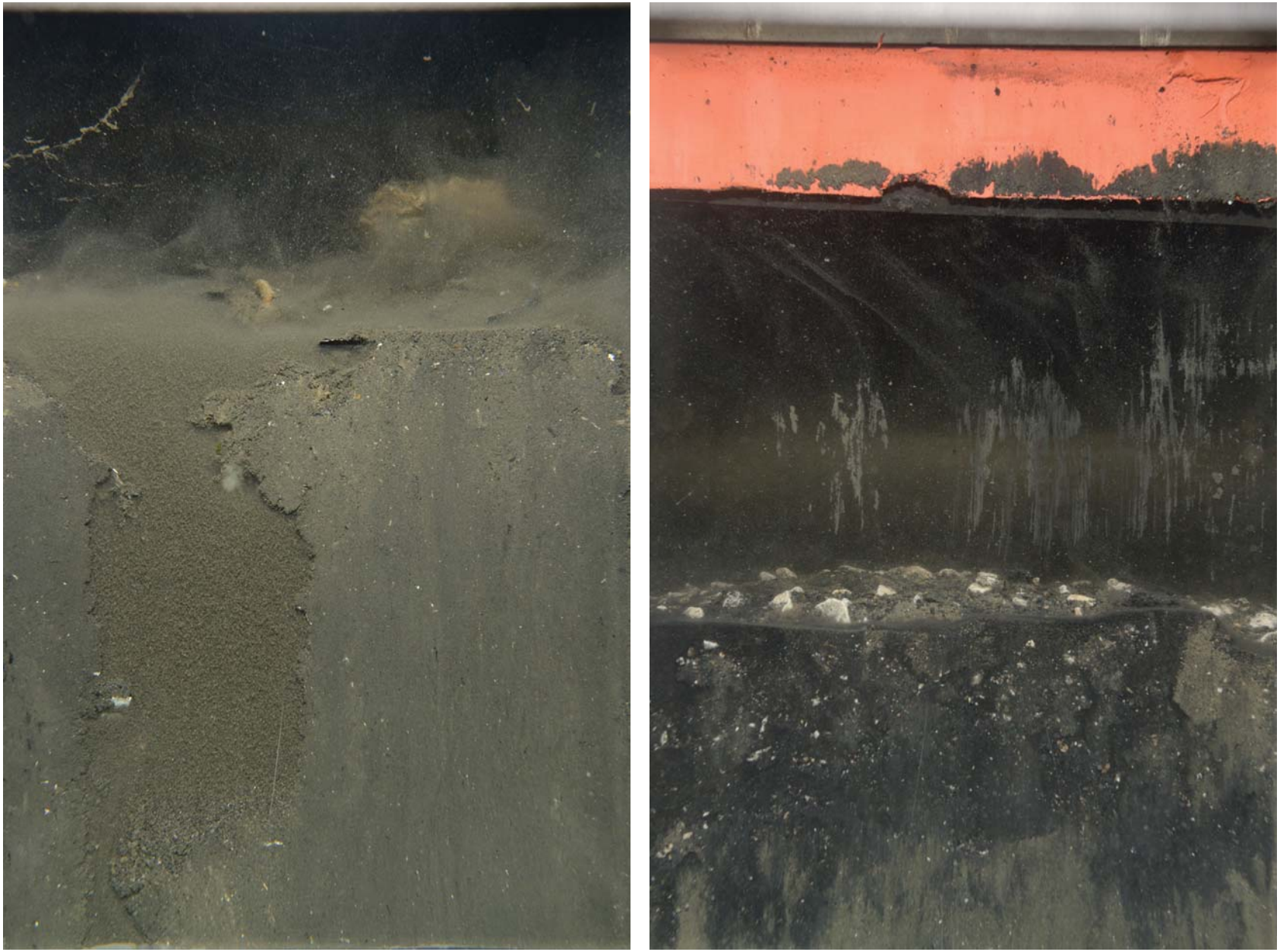

before **after**

Figure 6: These profile images from Station 3-4 taken before (left) and after (right) cap placement show the effects of cap placement on camera prism penetration depth. Scale: width of each image = 14.5 cm.

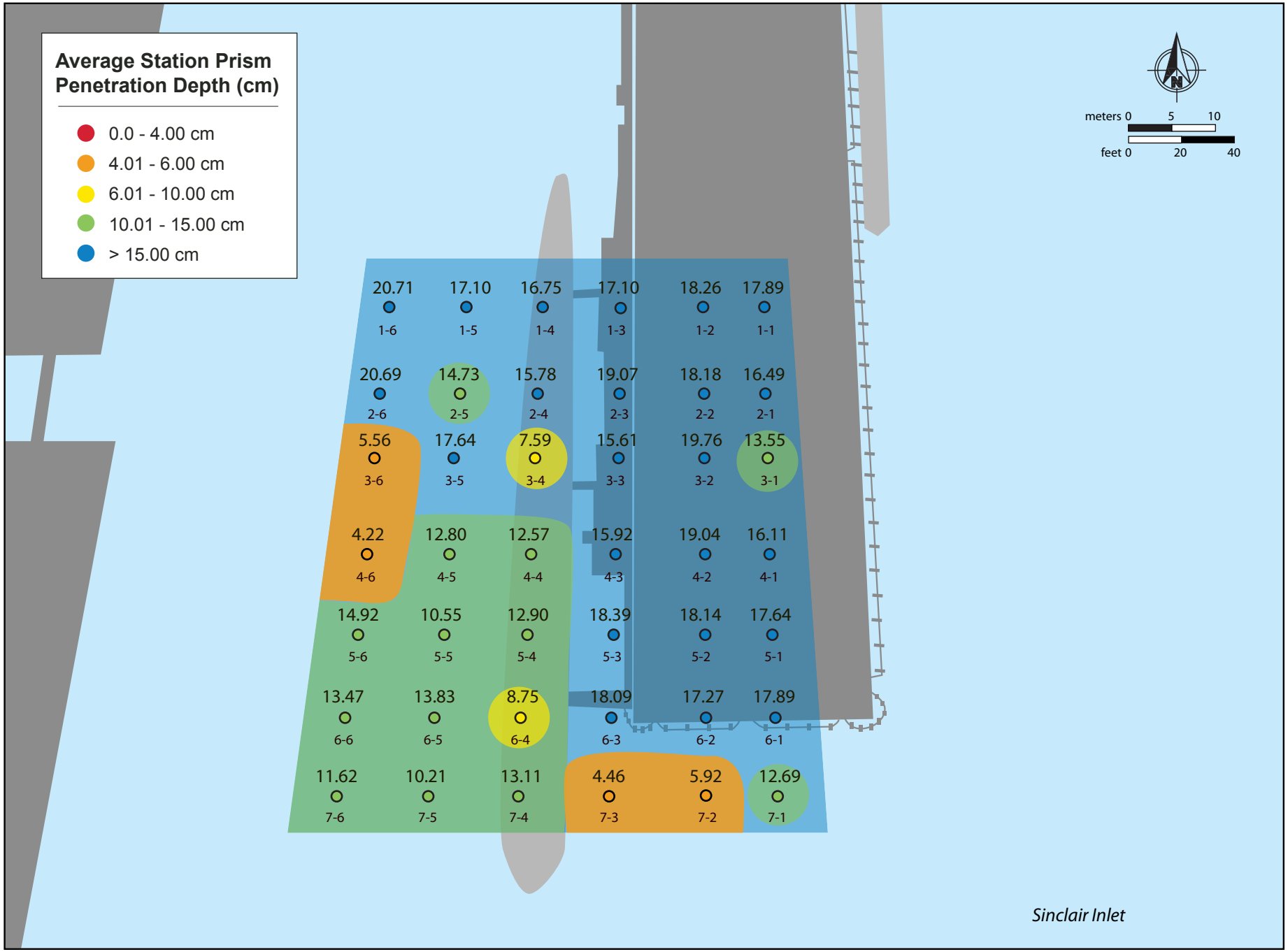

Figure 7: Spatial distribution of mean camera prism penetration depth (cm) at Pier 7 at the PSNS & IMF Bremerton site in October, 2012.

2-5

4-4

Figure 8: These profile images from Stations 2-5 (left) and 4-4 (right) show the difference between locations with just traces of AquaGate particles (left) versus those with a thicker deposit (right). Scale: width of each image = 14.5 cm.

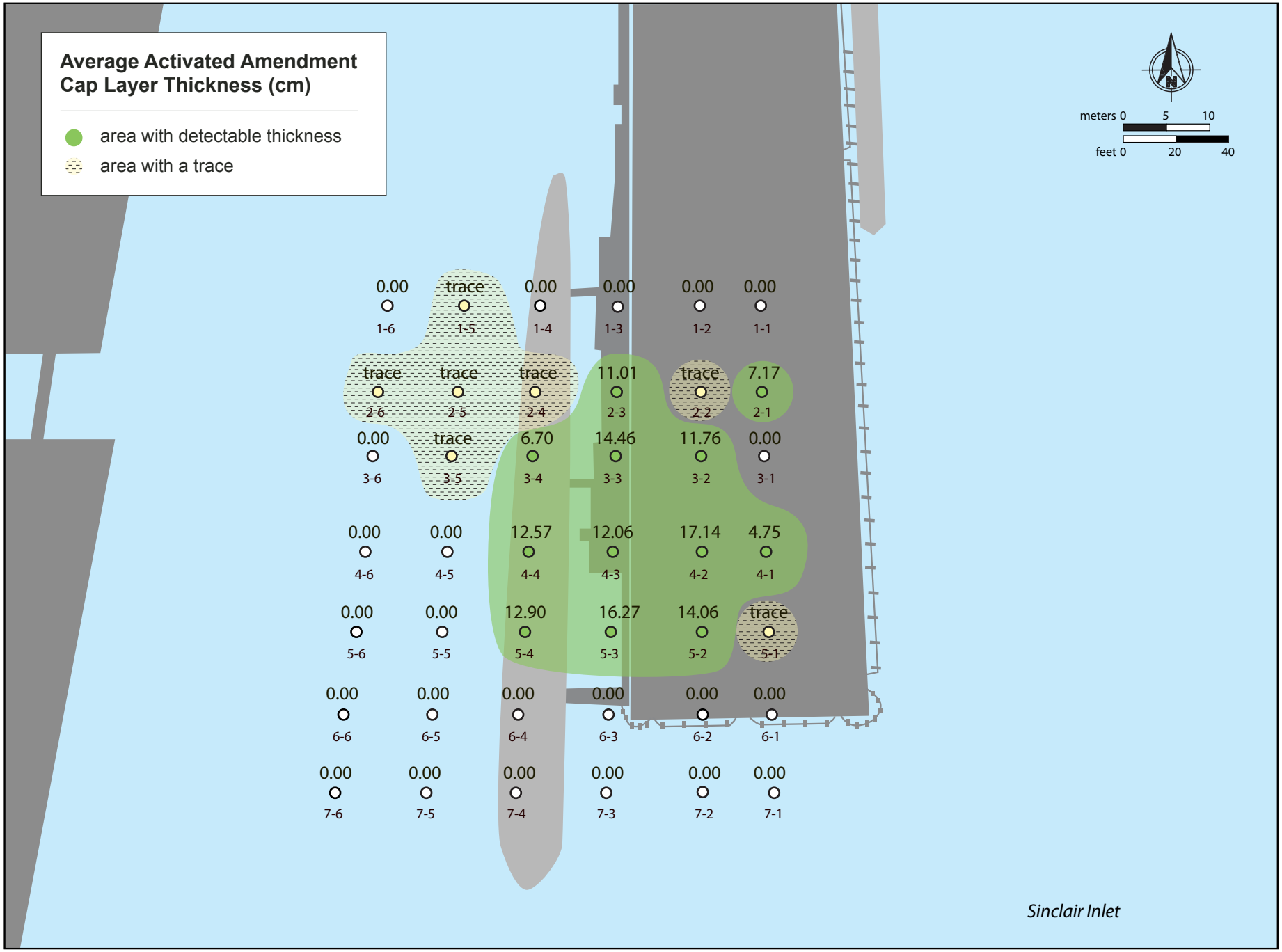

Figure 9: Spatial distribution and average depositional thickness (cm) of the AquaGate +PAC^{TM} material placed at locations in and around Pier 7 at the PSNS & IMF Bremerton site.

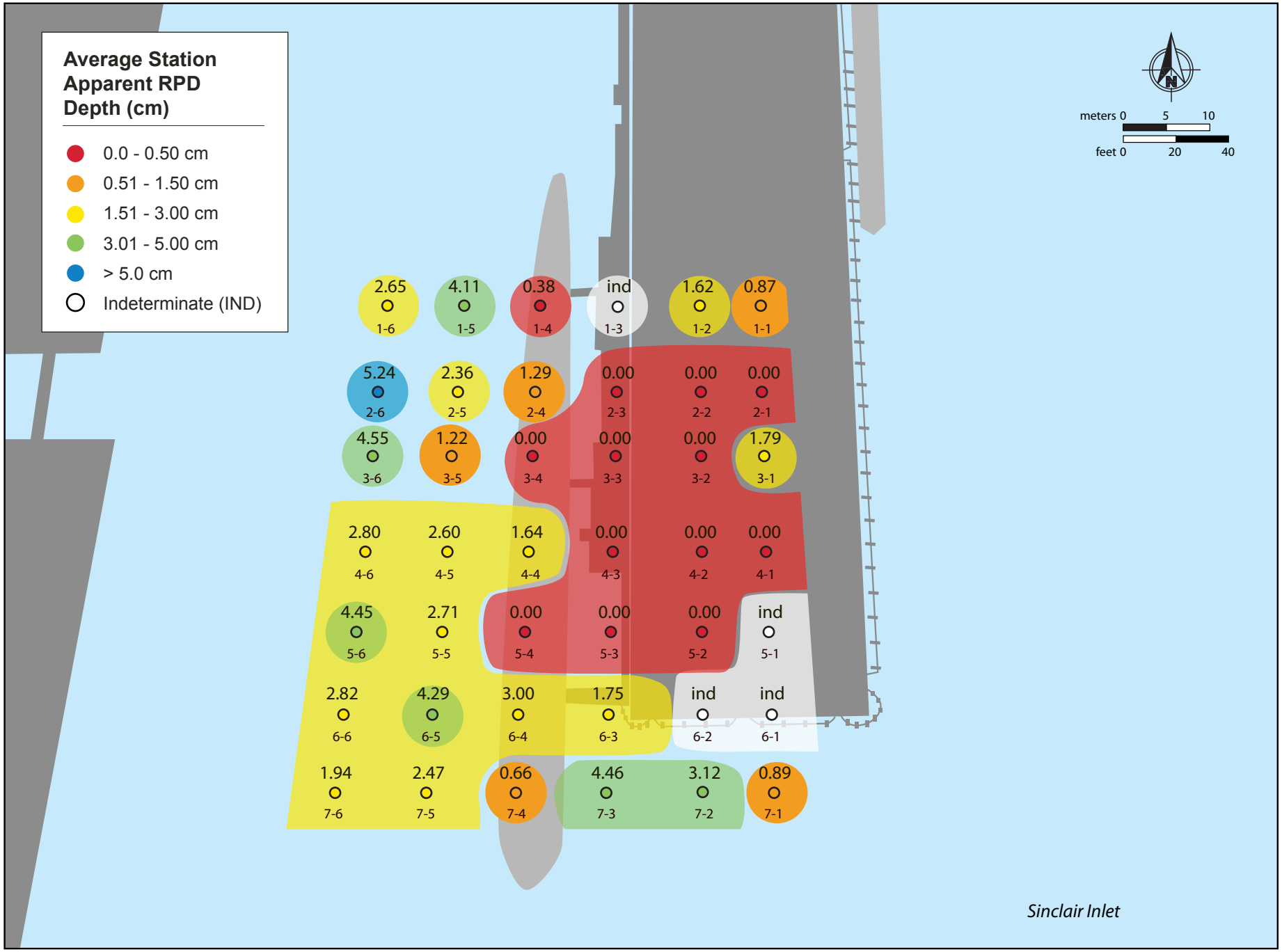

Figure 10: Spatial distribution of mean apparent RPD depth (cm) at Pier 7 at the PSNS & IMF Bremerton site in October, 2012.

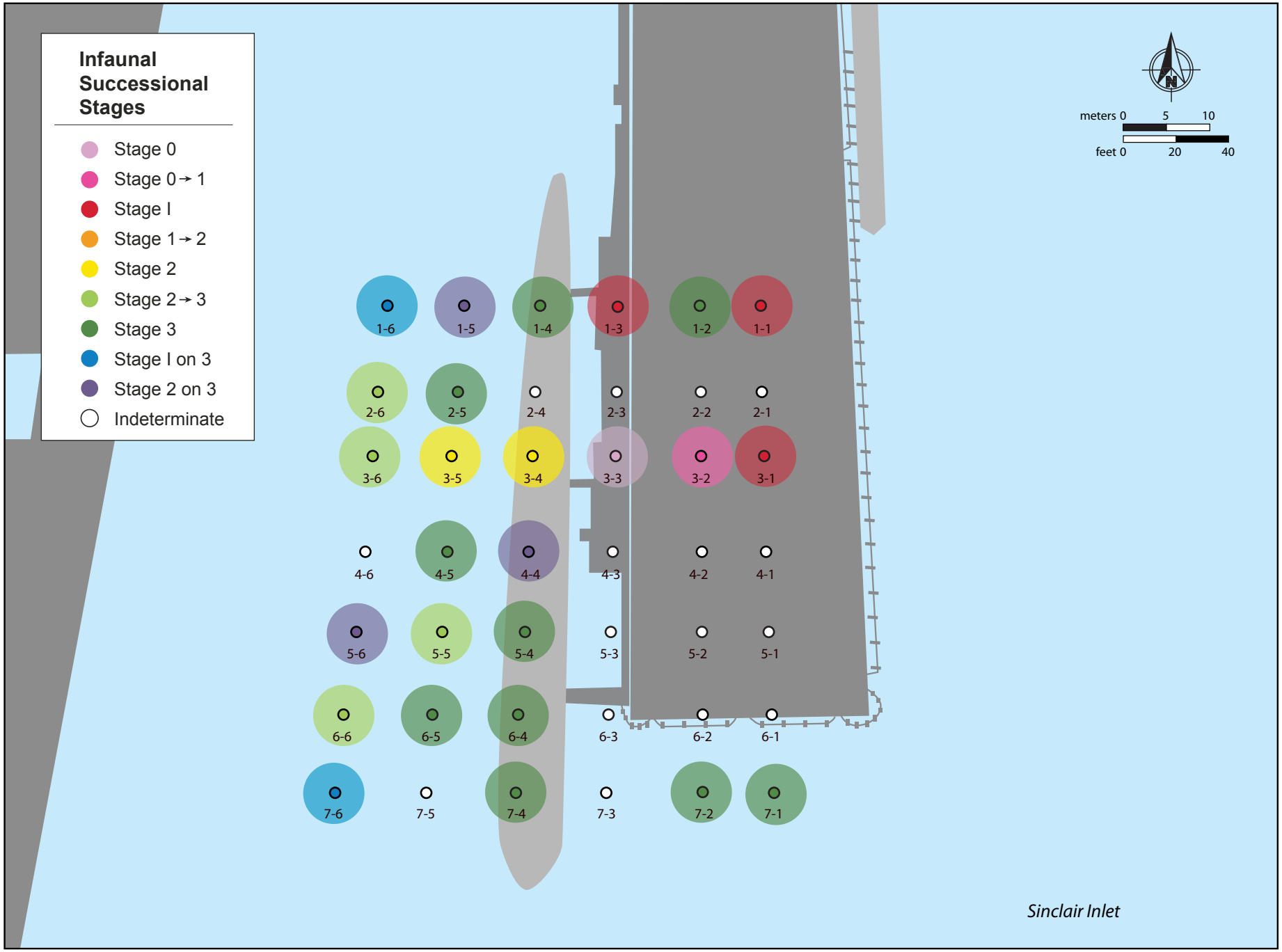

Figure 11: Spatial distribution of infaunal successional stages at Pier 7 at the PSNS & IMF Bremerton site in October, 2012.

before **after**

Figure 12: These profile images from Station 5-4 taken before (left) and after (right) cap placement show how placement of the cap material eliminated the assemblage of large sabellid polychaete tubes that were present during the baseline survey. Scale: width of each image = 14.5 cm.

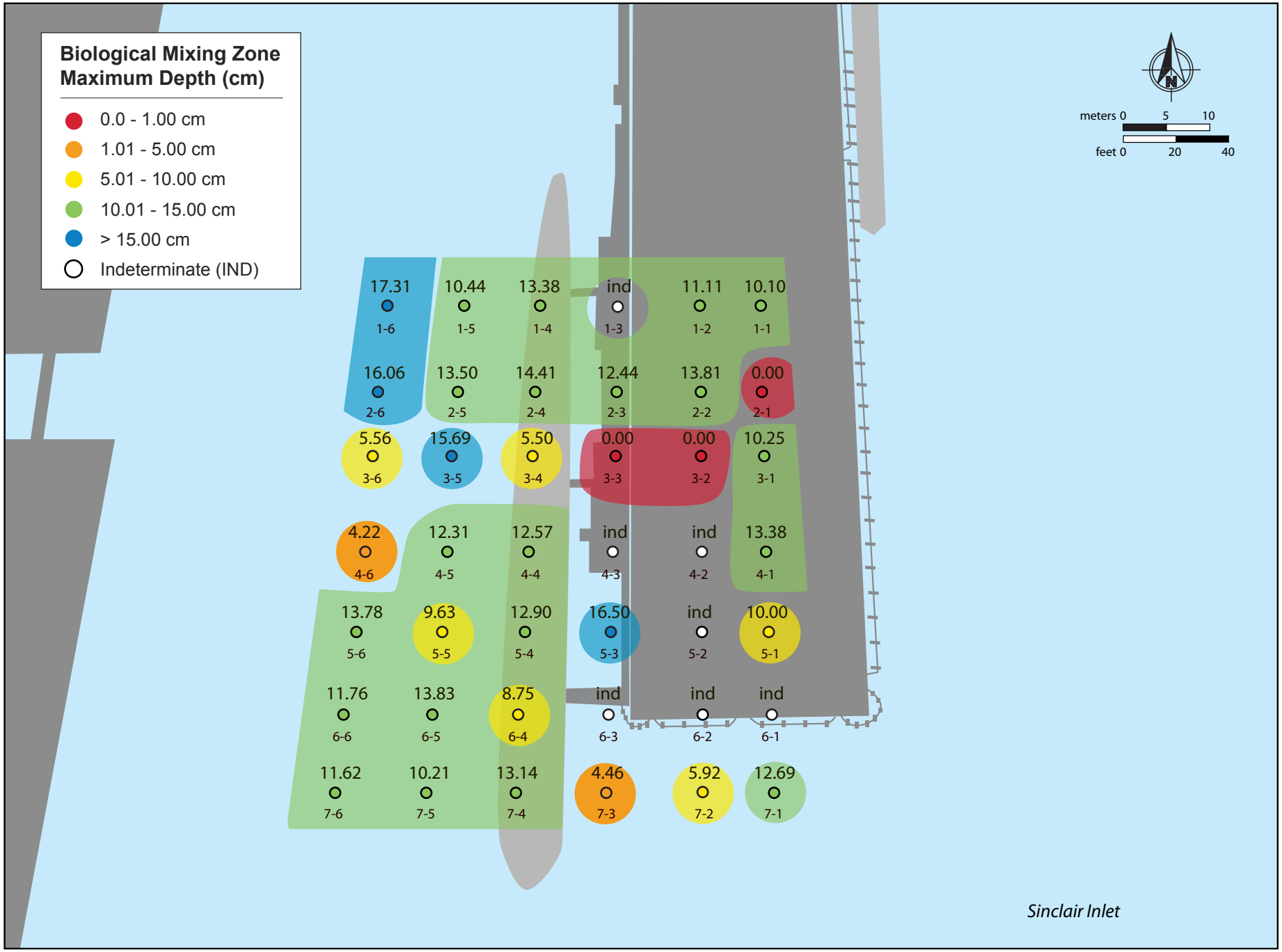

Figure 13: Spatial distribution of maximum biological mixing depth at Pier 7 at the PSNS & IMF Bremerton site in October, 2012.

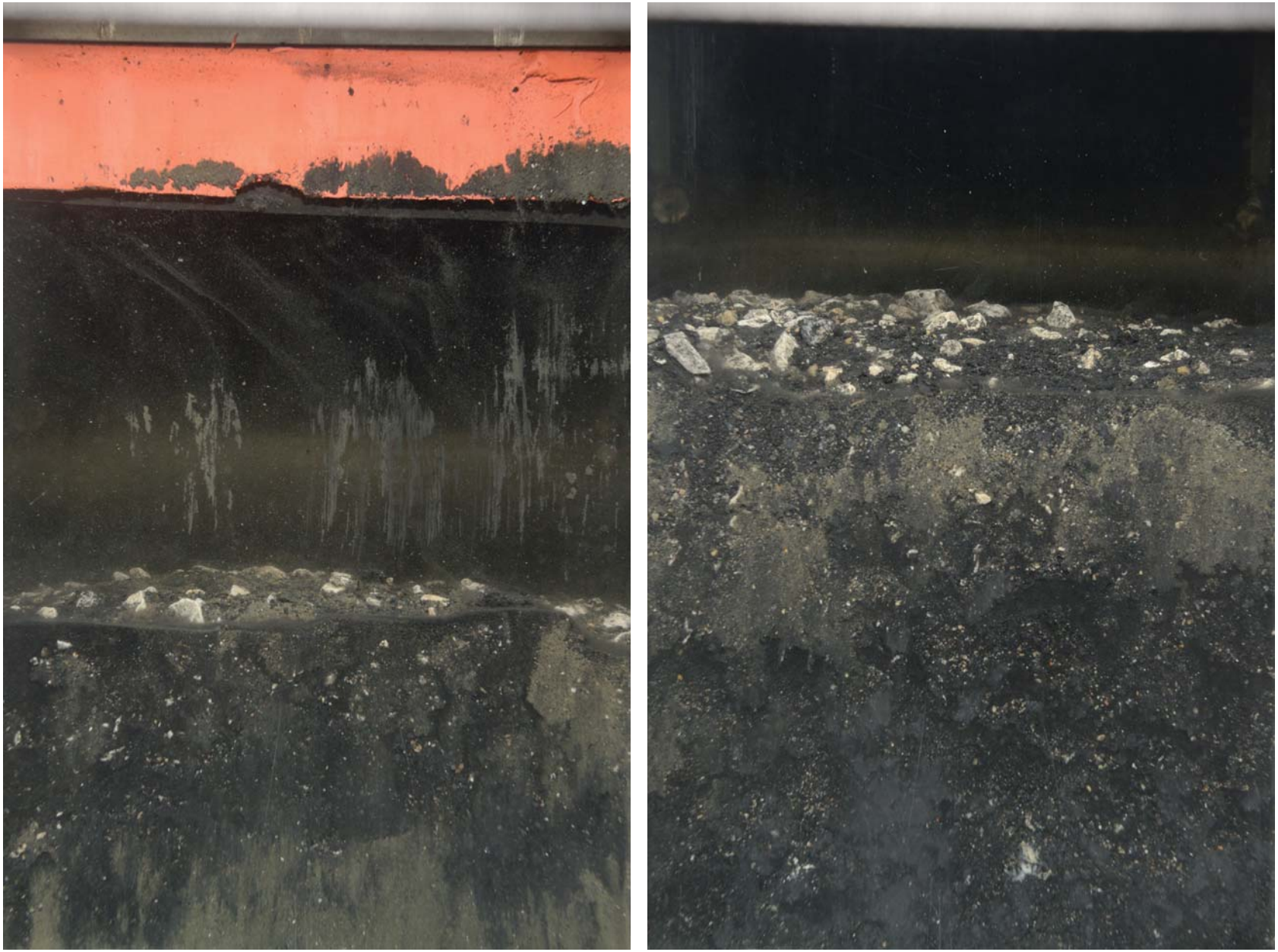

3-4 5-4

Figure 14: These profile images from Stations 3-4 (left) and 5-4 (right) show how the activated carbon covering on the carrier particles for the AquaGate+PAC™ has dissolved off the carrier granules, leaving a surface armoring of white pebbles while the carbon particles are being re-worked throughout the underlying sediment column. Scale: width of each image = 14.5 cm.

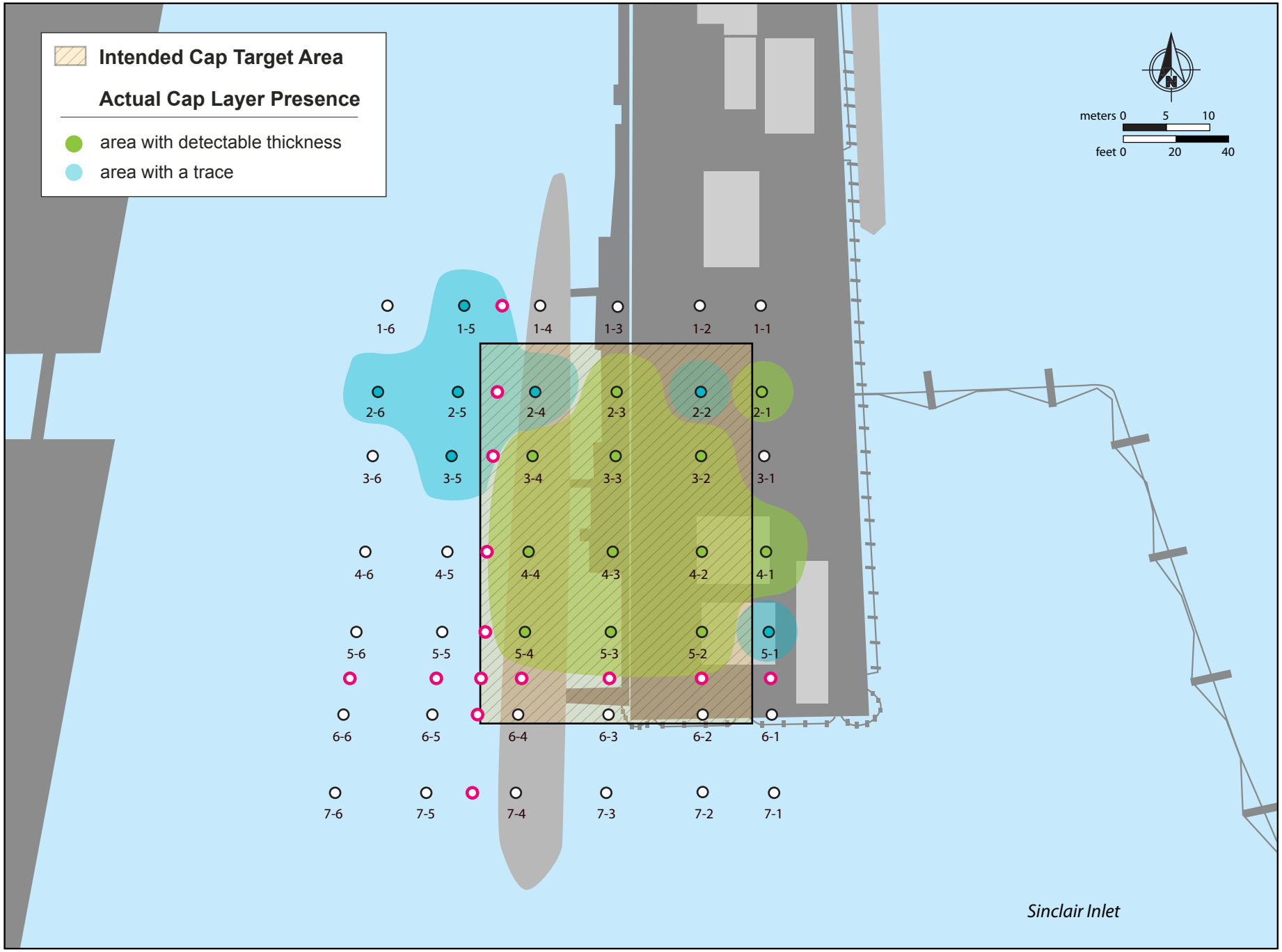

Figure 15: Comparison of the intended cap target area with the actual cap presence measured in the October 2012 SPI survey.

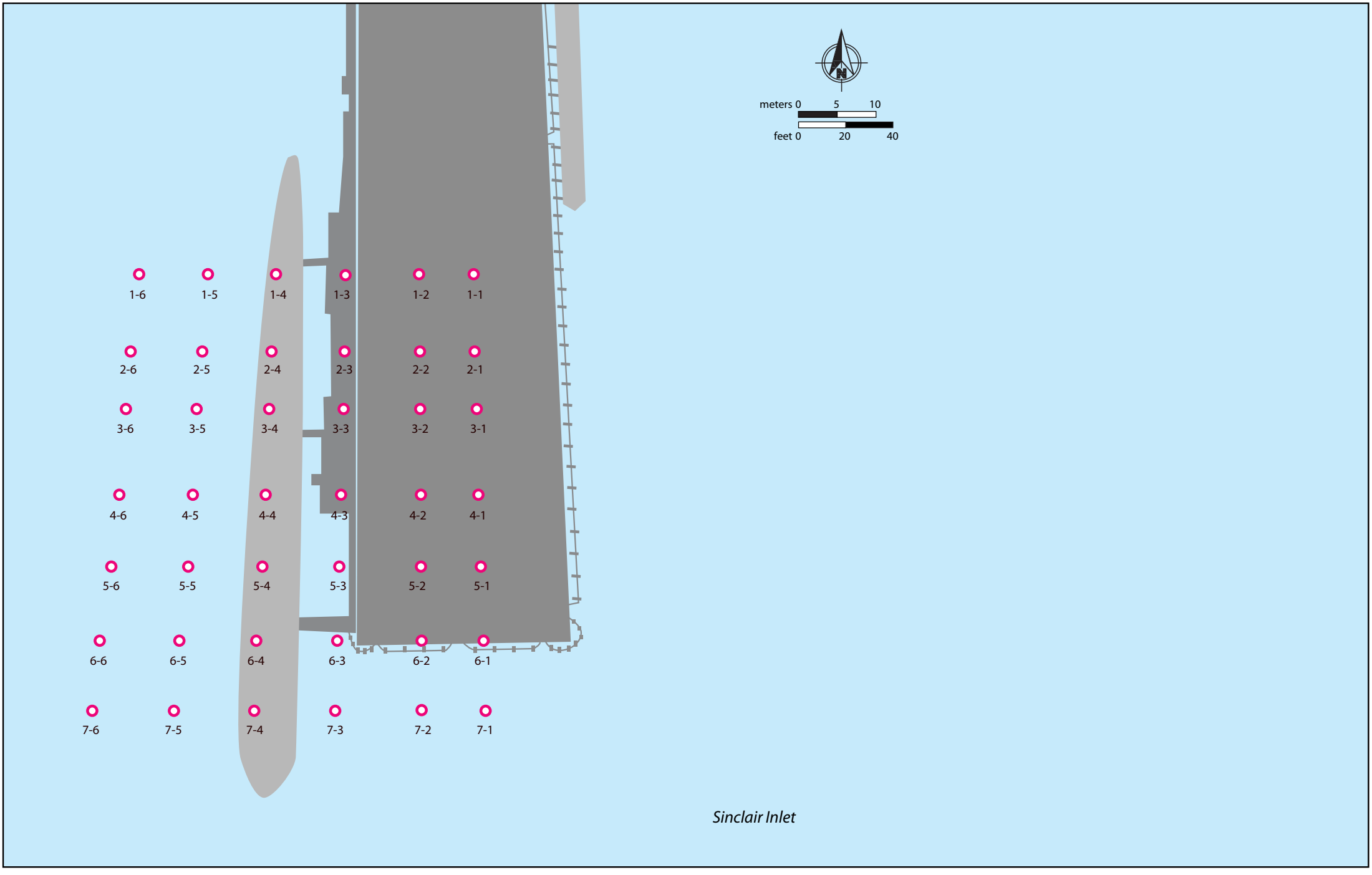
meters 0 5 10
feet 0 20 40
1-6
1-5
1-4
1-3
1-2
1-1
2-6
2-5
2-4
2-3
2-2
2-1
3-6
3-5
3-4
3-3
3-2
3-1
4-6
4-5
4-4
4-3
4-2
4-1
5-6
5-5
5-4
5-3
5-2
5-1
6-6
6-5
6-4
6-3
6-2
6-1
7-6
7-5
7-4
7-3
7-2
7-1
Sinclair Inlet

APPENDIX A

Sediment Profile Image Analysis Results

STATION	Frame or Hand-Held	REP	DATE	TIME	Calibration Constant	Penetra-tion Area (sq.cm)	Average Penetration (cm)	GAC Layer Area (sq.cm)	Mean GAC Layer depth (cm)	RPD Area (sq.cm)	Mean RPD (cm)	Mixing Zone Max Depth (cm)	Successional Stage	COMMENT
T 1-1	H	C	10/31/2012	7:09:40	14.5995	261.14	17.89	0.00	0.00	12.77	0.87	10.10	Stage 1	depth; no GAC present
T 1-2	H	E	10/31/2012	7:16:45	14.5995	266.59	18.26	0.00	0.00	23.72	1.62	11.11	Stage 3	Sandy silt; SWI covered with med-sized shell frag, smaller shell fragments incorporated in upper 10cm; large polychaete at depth; no GAC layer
T 1-3	H	B	10/30/2012	15:17:24	14.5995	249.67	17.10	0.00	0.00	ind	ind	ind	Stage 1	Silt-clay with minor fine sand fraction, thin layer of shell fragments on surface in background, incorporated through depth; aRPD and cross-sectional integrity compromised by diver insertion & disturbance; no GAC layer present
T 1-4	F	A	10/31/2012	14:51:45	14.5131	243.05	16.75	0.00	0.00	5.55	0.38	13.38	Stage 3	Silt-clay with patches of Beggiatoa at surface; patchy, discontinuous aRPD; sabellid tube on surface; low 02 in benthic boundary layer.
T 1-5	F	A	10/31/2012	14:32:34	14.5131	248.25	17.10	0.00	trace	59.60	4.11	10.44	Stage 2 on 3	Silt-clay with traces of GAC; void at base of aRPD
T 1-6	F	B	10/31/2012	14:40:42	14.5131	300.58	20.71	0.00	0.00	38.49	2.65	17.31	Stage 1 on 3	Silt-clay with minor very fine sand fraction, evidence of subsurface burrowing throughout profile.
T 2-1	H	F	10/31/2012	7:02:56	14.5995	240.82	16.49	104.72	7.17	0.00	0.00	0.00	indeterminate	GAC layer dominate in upper 6-7 cm, incorporated in bits with sediment through rest of depth; surface layer of shell frag, fine structure in profile eliminated from diver sampling artifact, impossible to determine successional stage or max BMD
T 2-2	H	B	10/30/2012	14:42:55	14.5995	265.43	18.18	trace	trace	0.00	0.00	13.81	indeterminate	Sandy silt with organic debris and shell fragments at surface; uneven surface; very small patches of oxy sed and GAC both at SWI and at depth; cross sectional sedimentary structure disturbed/destroyed by diver prism vibration.
T 2-3	H	A	10/30/2012	14:51:23	14.5995	278.48	19.07	160.74	11.01	0.00	0.00	12.44	indeterminate	GAC layer most of depth, up to 11cm, small shell fragments throughout and a few on surface; silty sed with shell fragments below GAC to depth, cross-sectional detail obliterated by diver sampling artifact
T 2-4	F	B	10/31/2012	13:59:34	14.5131	229.01	15.78	trace	trace	18.76	1.29	14.41	indeterminate	Disturbance at SWI and burrow on right edge appear to be caused by artifact dragdown of bivalve shell; traces of small GAC particles within oxidized surface layer, but no distinct deposit present.
T 2-5	F	A	10/31/2012	14:11:18	14.5131	213.79	14.73	trace	trace	34.32	2.36	13.50	Stage 3	Very fine sandy silt with traces of GAC particles in surface oxidized layer; some particles dragged to depth; appears that just a few mm dusting of particles originally landed in this location, no distinct deposit.
T 2-6	F	B	10/31/2012	14:19:01	14.5131	300.21	20.69	trace	trace	76.01	5.24	16.06	Stage 2 -> 3	Silt clay with faintest trace of GAC particles (< 50) sprinkled throughout oxidized layer, less than at Station 2-5; evidence of subsurface burrowing.
T 3-1	H	A	10/30/2012	14:19:44	14.5995	197.80	13.55	0.00	0.00	26.12	1.79	10.25	Stage 1	Very fine sandy silt with organic debris on surface and shell fragments throughout profile; fine structure of profile obliterated by diver artifact, a few grains of GAC visible but no distinct deposit.
T 3-2	H	A	10/30/2012	14:26:45	14.5995	288.52	19.76	171.66	11.76	0.00	0.00	0.00	Stage 0	GAC layer upper 12 cms, more to the right, sediment at depth and more to left at an angle; as with other hand-held shots, there is a smear from camera, and diver insertion at angle along with prism wiggling is distorting any stratigraphy that was present.
T 3-3	H	B	10/30/2012	14:31:43	14.5995	227.97	15.61	211.13	14.46	0.00	0.00	0.00	Stage 0 -> 1	GAC layer throughout almost all of depth, GAC carrier pebbles visible on surface; as with other diver samples, profile stratigraphy distorted by sampling artifact.
T 3-4	F	C	10/31/2012	11:08:07	14.5131	110.16	7.59	97.21	6.70	0.00	0.00	5.50	Stage 2	GAC layer throughout depth; carrier vehicle pebbles visible on surface, evidence of subsurface burrowing.
T 3-5	F	C	10/31/2012	10:53:40	14.5131	256.00	17.64	trace	trace	17.68	1.22	15.69	Stage 2	Very fine sandy silt with traces of GAC particles in surface oxidized layer; some particles dragged to depth; appears that just a few mm dusting of particles originally landed in this location, no distinct deposit.
T 3-6	F	A	10/31/2012	10:44:32	14.5131	80.70	5.56	0.00	0.00	65.97	4.55	5.56	Stage 2 -> 3	Compact silty sand; aRPD extends to base of image; small worms visible in upper cms of aRPD; no trace of GAC
T 4-1	H	C	10/30/2012	13:36:08	14.5995	235.23	16.11	69.29	4.75	0.00	0.00	13.38	indeterminate	GAC layer in upper 4-5 cms, patchy in depth; GAC carrier residuals and shells at surface; shell fragments incorporated throughout profile, fine-scale stratigraphy compromised by diver sampling artifact.
T 4-2	H	A	10/30/2012	13:39:45	14.5995	278.03	19.04	250.27	17.14	0.00	0.00	ind	indeterminate	GAC layer throughout most of depth; GAC carrier pebbles on surface; biogenic structure and sediment stratigraphy destroyed by diver sampling artifact.
T 4-3	H	A	10/30/2012	13:42:33	14.5995	232.46	15.92	176.12	12.06	0.00	0.00	ind	indeterminate	GAC layer throughout most of depth; GAC carrier pebbles on surface, shell fragments in upper cms; biogenic and sediment stratigraphy not preserved due to diver-induced artifacts.
T 4-4	F	B	10/31/2012	10:10:15	14.5131	182.44	12.57	182.44	12.57	23.74	1.64	12.57	Stage 2 on 3	GAC layer incorporated throughout entire depth, mixed with sed in upper 4 cms, thin GAC layer along SWI too along with carrier pebbles; represents ideal outcome.
T 4-5	F	C	10/31/2012	10:22:30	14.5131	185.83	12.80	0.00	0.00	37.74	2.60	12.31	Stage 3	Silty very fine sand, coarser grains near surface; large open burrow to void from SWI to <8cm depth, some trace of GAC particles in oxidized layer.
T 4-6	F	B	10/31/2012	10:27:18	14.5131	61.28	4.22	0.00	0.00	40.65	2.80	4.22	indeterminate	Consolidated silty very fine sand, small worms near base of image; not enough penetration to determine successional stage; traces of individual GAC particles in surface oxidized layer.
T 5-1	H	A	10/30/2012	13:18:13	14.5995	257.49	17.64	trace	trace	ind	ind	10.00	indeterminate	Very fine sandy silt with large shells, including mussel shells, on surface; small shell fragments incorporated in upper 7 cm; biogenic structure & fine-scale stratigraphy destroyed by diver sampling artifacts.
T 5-2	H	D	10/31/2012	7:47:14	14.5995	264.89	18.14	205.31	14.06	0.00	0.00	ind	indeterminate	GAC layer throughout most of depth; GAC carrier pebbles visible on surface, biogenic structure and sediment stratigraphy compromised by diver sampling artifact.
T 5-3	H	A	10/30/2012	13:24:38	14.5995	268.52	18.39	237.46	16.27	0.00	0.00	16.50	indeterminate	GAC layer throughout most of depth; GAC carrier pebbles on surface; evidence of subsurface burrowing visible even though much of stratigraphy is compromised by diver artifact.
T 5-4	F	B	10/31/2012	11:49:38	14.5131	187.21	12.90	187.21	12.90	0.00	0.00	12.90	Stage 3	GAC layer throughout image, GAC carrier pebbles on surface; traces of buried sabellids at depth; GAC layer exceeds prism penetration depth.
T 5-5	F	A	10/31/2012	11:32:27	14.5131	153.17	10.55	0.00	0.00	39.27	2.71	9.63	Stage 2 -> 3	Very fine sandy silt with a few GAC particles in oxidized layer; sabellid tubes on surface; largely undisturbed since baseline.
T 5-6	F	C	10/31/2012	11:26:31	14.5131	216.60	14.92	0.00	0.00	64.59	4.45	13.78	Stage 2 on 3	Very fine sandy silt with a layer of coarser grains in upper cm, esp. on right; fauna above SWI in background; small worms below aRPD on left and at depth on right
T 6-1	H	A	10/30/2012	12:53:38	14.5995	261.20	17.89	0.00	0.00	ind	ind	ind	indeterminate	Silty sediment with lots of shell fragments incorporated throughout depth and on surface, biogenic and sedimentary structure compromised by diver sampling artifacts.

STATION	Frame or Hand-Held	REP	DATE	TIME	Calibration Constant	Penetra-tion Area (sq.cm)	Average Penetration (cm)	GAC Layer Area (sq.cm)	Mean GAC Layer depth (cm)	RPD Area (sq.cm)	Mean RPD (cm)	Mixing Zone Max Depth (cm)	Successional Stage	COMMENT
T 6-2	H	A	10/30/2012	12:56:54	14.5995	252.16	17.27	0.00	0.00	ind	ind	ind	indeterminate	Silty sediment with lots of shell fragments incorporated throughout depth and on surface, biogenic and sedimentary structure compromised by diver sampling artifacts.
T 6-3	H	A	10/30/2012	13:01:15	14.5995	264.08	18.09	0.00	0.00	25.49	1.75	ind	indeterminate	Silty sediment with lots of shell fragments incorporated throughout depth and on surface, biogenic and sedimentary structure compromised by diver sampling artifacts.
T 6-4	F	A	10/31/2012	9:33:45	14.5131	127.03	8.75	0.00	0.00	43.61	3.00	8.75	Stage 3	Very fine sandy silt with traces of GAC particles in surface oxidized layer; sabellid tubes at surface, evidence of subsurface burrowing.
T 6-5	F	B	10/31/2012	9:49:33	14.5131	200.65	13.83	0.00	0.00	62.26	4.29	13.83	Stage 3	Very fine sandy silt with large burrow/pit at center to ~6.2 cm; no trace of GAC layer.
T 6-6	F	B	10/31/2012	9:55:07	14.5131	195.44	13.47	0.00	0.00	40.87	2.82	11.76	Stage 2 -> 3	Very fine sandy silt with minimal trace of GAC particles, evidence of subsurface burrowing, profile similar to baseline image.
T 7-1	F	B	10/31/2012	8:27:09	14.5131	184.23	12.69	0.00	0.00	12.96	0.89	12.69	Stage 3	Very fine sandy silt with coarser grains near SWI; bivalve shell dragged down by prism blade creating large burrow artifact; no GAC particles
T 7-2	F	A	10/31/2012	8:35:21	14.5131	85.89	5.92	0.00	0.00	45.25	3.12	5.92	Stage 3	Poorly sorted medium to coarse sand with partially submerged crab against faceplate; no GAC present.
T 7-3	F	A	10/31/2012	8:42:06	14.5131	64.79	4.46	0.00	0.00	64.79	4.46	4.46	indeterminate	Sand, coarse grains, shell fragments on surface; rocks and algae on surface
T 7-4	F	A	10/31/2012	8:59:40	14.5131	190.21	13.11	0.00	0.00	9.55	0.66	13.14	Stage 3	Radical shift in grain size compared to previous stations in this row; silt-clay with old sabellid tubes on surface; anemone(s) at SWI and dragged to depth by prism blade.
T 7-5	F	A	10/31/2012	9:09:52	14.5131	148.19	10.21	0.00	0.00	35.82	2.47	10.21	indeterminate	Sandy silt with profile disturbed by prism dragging anemone to depth; most likely Stage 2 or 3 present.